*remote sensing*

MDPI

*Article*

# Spatiotemporal Comparison and Validation of Three Global-Scale Fractional Vegetation Cover Products

**Duanyang Liu [1,2], Kun Jia [1,2,*], Xiangqin Wei [3], Mu Xia [1,2], Xiwang Zhang [4], Yunjun Yao [1,2], Xiaotong Zhang [1,2] and Bing Wang [1,2]**

1 State Key Laboratory of Remote Sensing Science, Faculty of Geographical Science, Beijing Normal University, Beijing 100875, China; duanyangliu0505@mail.bnu.edu.cn (D.L.); xiamu@mail.bnu.edu.cn (M.X.); boyyunjun@bnu.edu.cn (Y.Y.); xtngzhang@bnu.edu.cn (X.Z.); icebergwb1995@mail.bnu.edu.cn (B.W.)

2 Beijing Engineering Research Center for Global Land Remote Sensing Products, Faculty of Geographical Science, Beijing Normal University, Beijing 100875, China

3 Institute of Remote Sensing and Digital Earth, Chinese Academy of Sciences, Beijing 100101, China; weixq@radi.ac.cn

4 Key Laboratory of Geospatial Technology for Middle and Lower Yellow River Regions (Henan University), Ministry of Education, Kaifeng 475004, China; zhangxiwang@vip.henu.edu.cn

* Correspondence: jiakun@bnu.edu.cn; Tel.: +86-10-5880-0152

Received: 2 September 2019; Accepted: 25 October 2019; Published: 29 October 2019

check for updates

**Abstract:** Fractional vegetation cover (FVC) is an important parameter for many environmental and ecological models. Large-scale and long-term FVC products are critical for various applications. Currently, several global-scale FVC products have been generated with remote sensing data, such as VGT bioGEOphysical product Version 2 (GEOV2), PROBA-V bioGEOphysical product Version 3 (GEOV3) and Global LAnd Surface Satellite (GLASS) FVC products. However, studies comparing and validating these global-scale FVC products are rare. Therefore, in this study, the performances of three global-scale time series FVC products, including the GEOV2, GEOV3, and GLASS FVC products, are investigated to assess their spatial and temporal consistencies. Furthermore, reference FVC data generated from high-spatial-resolution data are used to directly evaluate the accuracy of these FVC products. The results show that these three FVC products achieve general agreements in terms of spatiotemporal consistencies over most regions. In addition, the GLASS and GEOV2 FVC products have reliable spatial and temporal completeness, whereas the GEOV3 FVC product contains much missing data over high-latitude regions, especially during wintertime. Furthermore, the GEOV3 FVC product presents higher FVC values than GEOV2 and GLASS FVC products over the equator. The main differences between the GEOV2 and GLASS FVC products occur over deciduous forests, for which the GLASS product presents slightly higher FVC values than the GEOV2 product during wintertime. Finally, temporal profiles of the GEOV2 and GLASS FVC products show better consistency than the GEOV3 FVC product, and the GLASS FVC product presents more reliable accuracy ($R^2$ = 0.7878, RMSE = 0.1212) compared with the GEOV2 ($R^2$ = 0.5798, RMSE = 0.1921) and GEOV3 ($R^2$ = 0.7744, RMSE = 0.2224) FVC products over these reference FVC data.

**Keywords:** global fractional vegetation cover; comparison; validation

## 1. Introduction

Fractional vegetation cover (FVC) is defined as the fraction of green vegetation seen from nadir, which can characterize the growth conditions and horizontal density of land surface live vegetation [1–5]. As a significant biophysical parameter involved in surface processes [6], the FVC is widely used for studies of the atmosphere, pedosphere, hydrosphere, ecology, and their interactions [7].

Thus, accurate and stable FVC products with regional and global scales are critical for related studies, such as those on climate change, numerical weather predictions, and land-surface processes [8,9].

Remote sensing technology is a feasible and reliable way for large-scale and long-term FVC generation due to its excellent ability to provide land surface observations. Currently, many FVC estimation algorithms have been developed based on remote sensing data, which can be divided into three major types: empirical methods, pixel unmixing models and machine learning methods [10,11]. Empirical methods build the statistical relationships between the FVC and vegetation indices or specific bands' reflectance through sufficient and reliable sample data. Empirical methods can achieve satisfactory accuracy at the regional scale with specific vegetation types. However, empirical methods become invalid over large-scale regions, in which the various vegetation types and land conditions increase uncertainties in the established relationships [10,12]. Pixel unmixing models assume that each pixel is composed of several components, and the fraction of vegetation composition is the corresponding FVC value of the pixel [6,12,13]. The dimidiate pixel model, as a widely used method of pixel unmixing models, assumes that each pixel can be divided into two parts: vegetation and non-vegetation [12,14]. However, the main limitation of pixel unmixing models is the determination of representative endmembers because of the complex land surface conditions and various spectral characteristics over a large scale [12,15,16]. Recently, machine learning methods have also been widely used to retrieve FVC values because of their computational efficiency and stable performances in nonlinear fitting [7]. Generally, machine learning methods estimate the FVC through training on a representative sample database containing pre-processed reflectance and corresponding simulated land surface parameters data [7]. Several algorithms of machine learning methods are proposed for FVC product generation over regional and global scales with satisfying results [1,10,12].

With these developed FVC estimation algorithms, some FVC products over regional and global scales are generated from remote sensing data, which are summarized in Table 1. Among these FVC products, CNES/POLDER data are generated based on empirical method, which establishes a statistical relationship between the FVC and the simulated reflectance data by means of a kernel-driven model [17,18]. However, the CNES/POLDER FVC product is only available for 1996, 1997, and 2003, which limits time-series designs and long-term earth-monitoring applications. The EUMETSAT/LSA SAF FVC is estimated through a probabilistic spectral mixture analysis method [6,19,20], which is provided with a 3-km spatial resolution and a daily temporal resolution [21]. Nevertheless, this product is only generated over Europe, Africa and South America, which limits its application for global-scale researches. For the Carbon Cycle and Change in Land Observational Products from an Ensemble of Satellites (CYCLOPES) FVC product, neural networks and PROSPECT + SAIL (PROSAIL) canopy radiative transfer model simulations are adopted for FVC estimation [22]. However, significant systematic underestimation was detected in the CYCLOPES FVC product by Verger [23,24]. The VGT bioGEOphysical product Version 1 (GEOV1) FVC algorithm is based on a neural network that treats the top-of-canopy normalized reflectances as input data and the corrected CYCLOPES FVC product as the expectant output values [24,25]. The GEOV1 FVC product is linearly correlated with the CYCLOPES FVC product [26], but the GEOV1 FVC product also has poor spatial continuity with a large amount of missing data over high-latitude regions [12]. In addition, the validation result indicates that the GEOV1 FVC product overestimates FVC values by up to 0.20 in croplands [12,27].

Considering the poor performance of the GEOV1 FVC product, a new version of the global FVC product, known as the VGT bioGEOphysical product Version 2 (GEOV2) FVC product, is proposed based on neural networks [28]. The GEOV2 FVC achieves better performance in terms of the spatiotemporal continuity and accuracy than the GEOV1 FVC product [29]. Additionally, to further improve the spatial resolution and maintain temporal continuity, the GEOV3 FVC product is produced using PROBA-V data with a 300 m spatial resolution, which adopts a neural network algorithm along with data filtering, gap filling and smoothing processes [30,31]. In addition, the Global LAnd Surface Satellite (GLASS) FVC product, under the support of China's National High Technology Research and

Development Program, has comparable accuracy and better spatiotemporal continuity compared with the GEOV1 FVC product [7,12,32].

For these existing FVC products, comparisons and validations, especially over global-scale and long-term FVC products, are crucial for their usage and improvement in land surface models [24]. Currently, several studies have been performed to evaluate and compare the performance of these FVC products. For example, Mu et al validated the GEOV1 FVC product over croplands in the Heihe study area, and the results indicated that the GEOV1 FVC product presented systematic overestimation up to approximately 0.2 [27]. Ding et al compared and validated GEOV1 and regional Australian MODIS FVC products over the Australian continent. The spatial comparisons showed that there were robust correlations between these two FVC products. Temporally consistent validation showed that GEOV1 and Australian MODIS FVC products had similar seasonal variation and different magnitudes over several biome types, such as sparse vegetation and open broadleaved deciduous forest [24].Additionally, the SEVIRI and MERIS FVC products were compared over Europe, as well as Africa, by García-Haro et al, and clear differences between the two products were observed over South Africa, where MERIS generally presented lower FVC values than SEVIRI FVC product [33]. As a whole, the aforementioned studies of FVC comparisons and validations are confined to the regional scale or short periods. Studies comparing and validating global and long-term FVC products are rare. However, long time series of global FVC products are crucial in climate and hydrologic modelling, natural hazards monitoring and soil erosion risk assessment [5,9,34]. For various applications, it is important to assess and validate the differences among these FVC products [24]. Therefore, the main objective of this study is to conduct spatiotemporal consistency comparisons and validations for three representative global-scale FVC products, including the GEOV2, GEOV3, and GLASS FVC products. Moreover, the accuracy of these three FVC products is validated through reference FVC data, which are processed by the Implementing Multi-scale Agricultural Indicators Exploiting Sentinels (IMAGINES) project.

**Table 1.** The major fractional vegetation cover (FVC) products and their characteristics [32].

| Products | Sensor | Methods | Spatial Resolution | Temporal Resolution | Spatial Coverage | Temporal Coverage | References |
|---|---|---|---|---|---|---|---|
| CNES/ POLDER | POLDER | Empirical model | 6 km | 10 days | Global | 1996-1997, 2003 | [17] |
| EUMETSAT/LSA SAF | SEVIRI | The dimidiate pixel model | 3km | Daily | Europe, Africa, South American | 2005-present | [21] |
| EP5/ CYCLOPES | SPOT VGT | Machine learning methods | 1/112° | 10days | Global | 1998-2007 | [22] |
| ESA/ MERIS | MERIS | Machine learning methods | 300m | Month/ 10days | Global | 2002-2012 | [35] |
| GEOV2 FVC | SPOT VGT, PROBA-V | Machine learning methods | 1/112° | 10 days | Global | 1999-present | [28,29] |
| GEOV3 FVC | PROBA-V | Machine learning methods | 300m | 10days | Global | 2014-present | [30] |
| GLASS FVC | MODIS | Machine learning methods | 500m | 8 days | Global | 2000-present | [12] |

## 2. Data

### 2.1. GEOV2 FVC Product

The GEOV2 FVC product was derived from SPOT/VEGETATION data from January 1999 to December 2013 and PROBA-V data from January 2014 by the Copernicus Global Land Service. The main purpose of GEOV2 FVC product generation was improving the GEOV1 FVC product in terms of accuracy and spatiotemporal continuity, especially at high-latitude and equatorial areas [28]. For GEOV2 FVC product generation, a neural network algorithm was adopted to obtain instantaneous FVC estimations [29,36,37]. Training samples were collected from the BELMANIP2 sites from VEGETATION data and the corrected CYCLOPES FVC product over the 2003–2007 period [29, 38]. After correcting for atmospheric effects by means of the SMAC model [39], the top-of-canopy daily reflectance data with three bands (red, NIR and SWIR) were acquired as input data for FVC estimation [29]. Then, multi-step outlier rejection processes were conducted to remove abnormal estimations, which might be contaminated by atmospheric effects, such as clouds, aerosols, water vapor and ozone [40,41]. Finally, dedicated temporal techniques, combining an adaptive Savitzky-Golay (SG) filter and an innovative climatology fitting method (Consistent Adjustment of the Climatology to Actual Observations, CACAO), were applied to ensure continuity and robustness of the estimated FVC data [28,40,41]. In addition, the GEOV2 FVC product was provided with 10-day temporal resolution and 1-km spatial resolution by the Copernicus Global Land Service (https://land.copernicus.eu/global/products/fcover). In this study, the GEOV2 FVC product from 2001 to 2016 was adopted for comparison and validation.

### 2.2. GEOV3 FVC Product

To maintain continuity and improve the spatial resolution of the GEOV2 FVC product, a new algorithm was employed to develop the GEOV3 FVC product using PROBA-V observation data under the IMAGINES project [30]. Similar to the GEOV2 FVC algorithm, a neural network algorithm was used for GEOV3 FVC estimation with the blue, red and NIR reflectance as input data. Because there was no available PROBA-V data when this algorithm was proposed, the training process was conducted based on SPOT/VEGETATION data, whose bands were close to PROBA-V data in the VIS-NIR channels [28,30]. In addition, the CYCLOPES FVC product was adopted as the reference FVC values for training samples in GEOV3 FVC algorithm development. Because of the systematic underestimation of the CYCLOPES FVC product, it had a maximum value of 0.6872 ($FVC_{CYCV31}(99\%) = 0.6872$), which corresponds to full vegetation coverage $FVC = 1$. To address this problem, a scaling factor was applied to the CYCLOPES FVC product to correct the underestimation (formula 1) [25,28,30]. Compared with GEOV2 FVC product generation, the main discrepancy for the GEOV3 FVC product was that the SWIR reflectance were abandoned as input data. Because SWIR band (700 m) had approximate twice spatial resolution than VIS-NIR bands (300-m) in PROBA-V data [30,42]. The GEOV3 FVC product from 2014 to 2016 was obtained from the Copernicus Global Land Service (https://land.copernicus.eu/global/products/fcover) and was used for comparison and validation in this study.

$$FVC_{training} = \frac{1}{0.6872} * FVC_{CYCV31} \tag{1}$$

where $FVC_{CYCV31}$ is the extracted FVC value from the CYCLOPES V3.1 product, and $FVC_{training}$ is the corresponding corrected FVC value used to train the neural network.

### 2.3. GLASS FVC Product

The GLASS FVC product used in this study was generated by Beijing Normal University, China [12,43,44]. In 2015, Jia et al proposed the GLASS FVC estimation algorithm based on general regression neural networks (GRNNs) for MODIS surface reflectance data with red and NIR bands, and this algorithm achieved comparable accuracy and better performance in terms of the spatial continuity compared with the GEOV1 FVC product [12]. However, the developed GRNN-based FVC estimation algorithm presented unsatisfactory computation efficiency: it usually took over one hour to generate FVC data for one MODIS tile. Therefore, in 2016, Yang et al proposed the multivariate adaptive regression splines (MARS) method for GLASS FVC generation that presented both adequate computational efficiency and comparable accuracy to the GRNN method [7]. Under the direct validation in an agricultural region, the GLASS FVC product was more accurate ($R^2$ = 0.86, RMSE = 0.087) than the GEOV1 FVC product ($R^2$ = 0.71, RMSE = 0.193) [27,45]. Moreover, the FVC time series data used for validation were consistent with the whole-crop growing characteristics [45]. The GLASS FVC product had an 8-day temporal resolution, a 500-m spatial resolution, and sinusoidal grid projection, which was released in 'HDF' format by the National Earth System Science Data Sharing Infrastructure, National Science & Technology Infrastructure of China (http://www.geodata.cn/thematicView/GLASS.html). In this study, the GLASS FVC product from 2001 to 2016 was used for comparison and validation.

### *2.4. Field Survey Based Reference Data and MODIS Land Cover Data*

To evaluate the performances of different FVC products, in-situ FVC measurements were acquired under the IMAGINES programme, which aimed to continue the innovation and development activities, as well as support the operations of the Copernicus Global Land service (http://fp7-imagines.eu/pages/services-and-products/ground-data.php). With this purpose, the ground FVC measurement data were collected and processed by the Earth Observation LABoratory (EOLAB) and/or local teams [46,47]. To obtain the reference data, digital hemispherical photographs were taken and processed for the ground FVC data over different vegetation types. Then, an empirical transfer function between the reflectance and ground FVC values was derived based on multiple robust regression for each site. Finally, reference FVC maps were produced using high-spatial-resolution data, such as Landsat-8 and FASat-C data. For kilometric biophysical product assessment, these high-spatial-resolution reference maps were averaged over an area of 3 km×3 km. Because of the accurate generation processes and containing various vegetation types around the world, the reference data had reliable accuracy and were representative to evaluate the performance of the FVC products. Considering the temporal coverage of the adopted FVC products, 29 reference samples were available during 2014-2016 (showed in Table 2) and adopted to perform the evaluation in this study. In addition, the RMSE values of each site were calculated using the ground FVC data and their corresponding estimates from transfer function, which indicated the uncertainty of these reference FVC data.

**Table 2.** Information of the reference data.

| Site Name | Country | Lat (°) | Lon (°) | DOY [(a)] | Year | Crop Type [(b)] | FVC | RMSE |
|---|---|---|---|---|---|---|---|---|
| LaReina_Cordoba_1 | Spain | 37.8189 | -4.8624 | 140 | 2014 | 2,6,8,12 | 0.297 | 0.120 |
| LaReina_Cordoba_2 | Spain | 37.7929 | -4.82668 | 140 | 2014 | 2,6,8,12 | 0.407 | 0.120 |
| Barrax-LasTiesas | Spain | 39.05437 | -2.10068 | 149 | 2014 | 2,3,4,5,6,8,12,13 | 0.367 | 0.060 |
| Albufera | Spain | 39.27437 | -0.31644 | 158 | 2014 | 1 | 0.180 | 0.076 |
| Albufera | Spain | 39.27437 | -0.31644 | 175 | 2014 | 1 | 0.350 | 0.125 |
| Albufera | Spain | 39.27437 | -0.31644 | 196 | 2014 | 1 | 0.590 | 0.120 |
| Albufera | Spain | 39.27437 | -0.31644 | 219 | 2014 | 1 | 0.740 | 0.128 |
| Albufera | Spain | 39.27437 | -0.31644 | 234 | 2014 | 1 | 0.800 | 0.100 |
| Pshenichne | Ukraine | 50.07657 | 30.23224 | 163 | 2014 | 2,3,4,6,7 | 0.550 | 0.120 |
| Pshenichne | Ukraine | 50.07657 | 30.23224 | 212 | 2014 | 2,3,4,6,7 | 0.680 | 0.070 |
| Ottawa | Canada | 45.3056 | -75.7673 | 159 | 2014 | 2,4,7 | 0.391 | 0.103 |
| Ottawa | Canada | 45.3056 | -75.7673 | 176 | 2014 | 2,4,7 | 0.480 | 0.006 |
| Ottawa | Canada | 45.3056 | -75.7673 | 187 | 2014 | 2,4,7 | 0.487 | 0.020 |
| Ottawa | Canada | 45.3056 | -75.7673 | 210 | 2014 | 2,4,7 | 0.786 | 0.005 |
| SanFernando | Chile | -34.7228 | -71.0019 | 19 | 2015 | 4,5,7,8,12 | 0.440 | 0.126 |
| Barrax-LasTiesas | Spain | 39.05437 | -2.10068 | 145 | 2015 | 2,3,4,5,6,8,12,13 | 0.268 | 0.130 |
| Barrax-LasTiesas | Spain | 39.05437 | -2.10068 | 203 | 2015 | 2,3,4,5,6,8,12,13 | 0.223 | 0.047 |
| Pshenichne | Ukraine | 50.07657 | 30.23224 | 174 | 2015 | 2,4,7 | 0.460 | 0.084 |
| Pshenichne | Ukraine | 50.07657 | 30.23224 | 188 | 2015 | 4,7 | 0.619 | 0.075 |
| Pshenichne | Ukraine | 50.07657 | 30.23224 | 204 | 2015 | 4,7 | 0.528 | 0.078 |
| AHSPECT-Meteopol | France | 43.57281 | 1.374512 | 173 | 2015 | 11 | 0.260 | 0.090 |
| AHSPECT-Peyrousse | France | 43.66623 | 0.21954 | 174 | 2015 | 2,6 | 0.380 | 0.090 |
| AHSPECT-Urgons | France | 43.6397 | -0.43396 | 174 | 2015 | 4 | 0.550 | 0.090 |
| AHSPECT-Creón D'armagnac | France | 43.9936 | -0.0469 | 175 | 2015 | 4,11 | 0.590 | 0.090 |
| AHSPECT-Condom | France | 43.97429 | 0.335969 | 176 | 2015 | 2,5,6 | 0.331 | 0.090 |
| AHSPECT-Savenès | France | 43.82422 | 1.174945 | 176 | 2015 | 2,6,7 | 0.286 | 0.090 |
| Collelongo | Italy | 41.85 | 13.59 | 189 | 2015 | 16 | 0.840 | 0.030 |
| Collelongo | Italy | 41.85 | 13.59 | 266 | 2015 | 16 | 0.860 | 0.040 |
| Maragua_UpperTana | Kenya | -0.77202 | 36.9742 | 68 | 2016 | 5, 14,15 | 0.580 | 0.130 |

[a] DOY: day of year; [b] The indexes of land cover types. 1: rice, 2: wheat, 3: barley, 4: corn, 5: tree plantation, 6: sunflower, 7: soybean, 8: alfalfa, 9: potato, 10: shrubs, 11: grass, 12: legumes, 13: pappaver, 14: tea, 15: coffee, 16: beech forest.

Moreover, the MODIS Land Cover Climate Modelling Grid Product (MCD12C1) was also used as the base map to evaluate the performance of the three FVC products over different vegetation types (https://e4ftl01.cr.usgs.gov/). MCD12C1 was provided at a 0.05° spatial resolution and an annual temporal resolution, and was aggregated and re-projected from the MODIS Land Cover Type

Product (MCD12Q1, 500-m spatial resolution, 8-day temporal resolution) [48,49]. The International Geosphere-Biosphere Programme (IGBP) classification system was adopted as the basic classes for further comparison and validation in this study.

## 3. Methodology

In this study, three global scale FVC products, including GEOV2, GEOV3, and GLASS FVC products, were selected for comparison and validation. According to [24] and [50], evaluation and comparison of different land surface parameter products were performed through three main aspects: spatial consistency, temporal consistency and accuracy validation, which drawn reasonable conclusions about the compared products. Thus, the designed methods in this study were mainly referred to these two studies. Because of the multiple spatiotemporal resolutions of these FVC products, it was inconvenient to conduct comparisons and analyses directly. Therefore, all three FVC products were first resampled to a 0.05° spatial resolution using bilinear interpolation, which has a trade-off between interpolation accuracy and computational efficiency [51]. Additionally, monthly averaged FVC data were also calculated using the resampled FVC products for further comparison.

To conduct the comparison in terms of spatial consistency, the monthly averaged FVC maps of the GEOV2, GEOV3, and GLASS FVC products in January and July of 2015, which showed the representative spatial patterns in winter and summer, were selected to present their spatial patterns and completeness. In addition, the difference maps between different FVC products were calculated to investigate their spatial discrepancies [24,50]. Furthermore, histograms of these pre-processed monthly FVC data from 2014 to 2016 over different vegetation types were generated according to the MODIS land cover product (MCD12C1, IGBP), which aimed to further explain the distribution patterns of the FVC values for different vegetation types [48].

In the temporal consistency comparison, temporal profiles of the mean values for different land cover types were calculated to determine the temporal consistency among these FVC products [24,51]. Moreover, several temporal profiles were extracted from the processed FVC data over the site locations in Table 2. Inter-annual and seasonal variations of these FVC products were analysed through these temporal profiles across different land conditions, as well as vegetation types. In addition, the reference FVC values were also added to the extracted temporal profiles for comparison. Furthermore, the accuracies of these three products were evaluated by direct comparison with the reference FVC data. In this study, these FVC products with original spatiotemporal resolutions were used for accuracy validation. Because the reference data were the averaged FVC values over a 3 km × 3 km region at each site, the mean values of 5 × 5 pixel subset at each site were adopted for the GLASS FVC product, the 3×3 pixel subset for the GEOV2 FVC product and the 9×9 pixel subset for the GEOV3 FVC product. The R-squared ($R^2$) value and root mean square error (RMSE) were used to quantify the uncertainty and accuracy of each FVC product.

$$R^2 = \frac{\sum_{i=1}^{n}\left(FVC_{\text{Product}(i)} - \overline{FVC_{\text{Product}}}\right)^2 - \sum_{i=1}^{n}\left(FVC_{\text{Product}(i)} - FVC_{\text{Reference}(i)}\right)^2}{\sum_{i=1}^{n}\left(FVC_{\text{Product}(i)} - \overline{FVC_{\text{Product}}}\right)^2}, \tag{2}$$

$$RMSE = \sqrt{\frac{\sum_{i=1}^{n}\left(FVC_{\text{Product}(i)} - FVC_{\text{Reference}(i)}\right)^2}{n}}, \tag{3}$$

where $n$ denotes the number of selected FVC values, which is 29 in this study; $FVC_{Product(i)}$ denotes the *ith* FVC value extracted from the sites in Table 2; $FVC_{Reference(i)}$ denotes the *ith* FVC value of the reference FVC data in Table 2; and $\overline{FVC_{Product}}$ denotes the mean value of the extracted FVC data from the corresponding product.

## 4. Results

### 4.1. Spatial Consistency

To compare the spatial consistency, the monthly FVC maps of the GEOV2, GEOV3, and GLASS FVC products in January and July of 2015 are shown in Figure 1. The dark grey areas represent missing data. Visually, the GLASS FVC products present excellent spatial completeness and no missing data were found, which is mainly attributed to the pre-processing procedure to obtain continuous and smooth reflectance data before the product generation process [12]. Additionally, the GEOV2 FVC product shows a significant improvement in the spatial completeness over the GEOV1 FVC product, the latter presenting approximately 20% missing data over the BELMANIP2 sites during 1999–2010 [52,53]. However, the GEOV3 FVC product presents poor spatial completeness because of a large fraction of missing values in the high-latitudes are found during winter. Figure 1 also shows a general agreement in the spatial distribution among these three FVC products. In January, high FVC values are mainly concentrated around the equator areas, such as north South America, Central Africa and Indonesia, where tropical and subtropical moist broadleaf forests are the dominant vegetation types [54]. In addition, North America, Asia and Europe have low FVC values. During summer, there is a clear increase in the FVC values in northern and eastern Asia, North America and Europe. Moreover, all three products show low FVC values during both winter and summer over the midwestern Qinghai-Tibet Plateau, the Himalayas and the Arabian Peninsula, which are mainly covered by desert scrublands or montane grasslands [54]. These spatial distributions of these FVC products are in accordance with the global terrestrial ecoregions and seasonal variations.

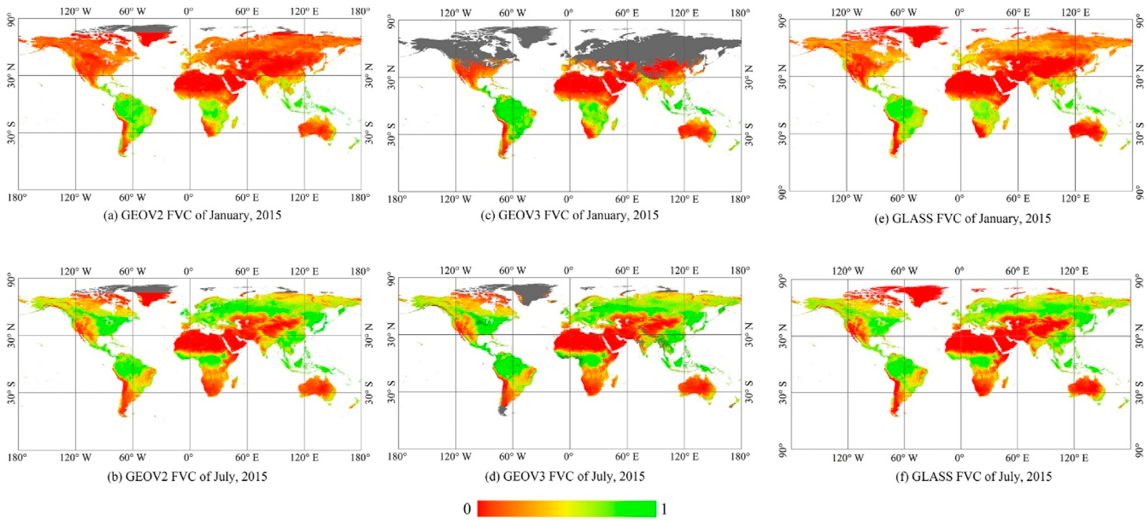


**Figure 1.** Monthly average global FVC maps from bioGEOphysical product Version 2 (GEOV2), bioGEOphysical product Version 3 (GEOV3), and Global LAnd Surface Satellite (GLASS) FVC products in January (**top**) and July (**bottom**), 2015.

To quantify the differences in these spatial patterns, the difference maps for these FVC products in January and July of 2015 are generated in Figure 2. Considering the poor spatial completeness of the GEOV3 FVC product, only pixels where both selected FVC products have valid FVC data are used to calculate the difference maps. With the negative values around the equator in Figure 2a–d, both the GEOV2 and GLASS FVC products show lower FVC values than the GEOV3 FVC product. For example, the GEOV3 FVC product presents approximately 0.15 and 0.13 larger than the GEOV2 and GLASS FVC values over the Amazon rain forest region. Generally, GLASS and GEOV2 show clear discrepancies across different hemispheres in January. Specifically, the GLASS FVC values are slightly higher than the GEOV2 FVC values in the Northern Hemisphere but lower in the Southern Hemisphere. In July, negative difference values between the GLASS and GEOV2 FVC products are found in Europe, Southwest Asia and southern North America. In addition, random signs for the difference values are observed over Europe between the GLASS and GEOV3 FVC products in July 2015.

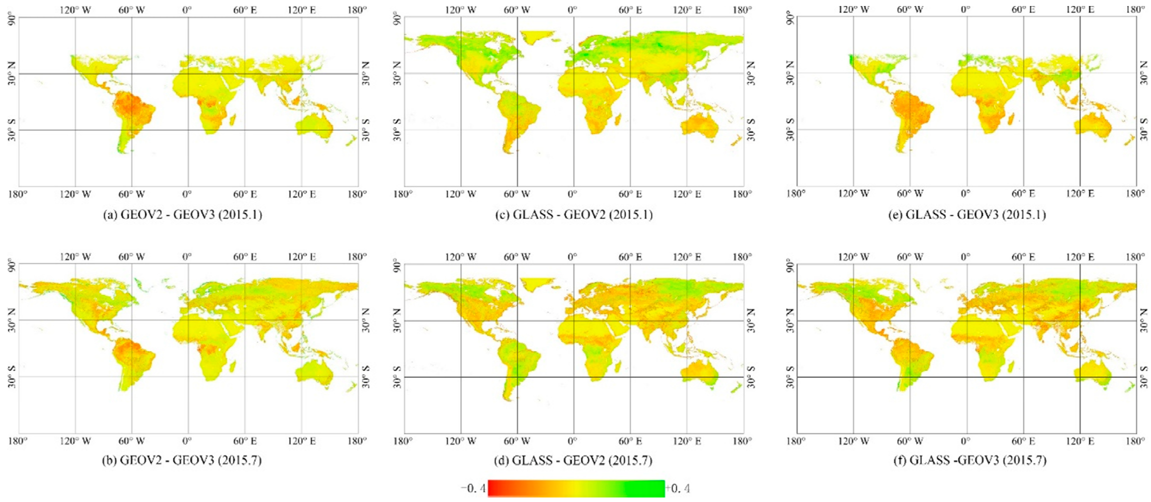


**Figure 2.** Difference maps among GEOV2, GEOV3, and GLASS FVC products in January (**top**) and July (**bottom**), 2015.

To further evaluate the spatial consistency of these three FVC products, the histograms of the GEOV2, GEOV3, and GLASS FVC values during 2014–2016 with different biome types are generated based on the MODIS land cover data and pre-processed monthly FVC products (Figure 3). Because there are some missing data in the GEOV3 product, only the pixels with available FVC values of all three products in the same period are adopted for statistical analysis. Additionally, several vegetation types, which are mainly distributed in high-latitudes, are also abandoned for further evaluation to avoid the disturbance of the missing data in GEOV3 FVC product (like Figure A1 in Appendix A), and finally the classes, including evergreen broadleaf forest, deciduous needleleaf forest, deciduous broadleaf forests, closed shrubland, grasslands, permanent wetlands, and croplands, as well as barren or sparsely vegetated, are used for further analysis. Generally, histograms of the three FVC products show excellent agreements over the adopted vegetation types, particularly in closed shrubland and croplands, where all three FVC products have similar distribution patterns. The spatial distributions for evergreen broadleaf forest of the GLASS and GEOV2 FVC products are more consistent than that of the GEOV3 FVC product. There were more pixels, which are concentrated between 0.6 and 0.95, in the GLASS and GEOV2 FVC products. In contrast, the GEOV3 FVC product has more pixels with higher values close to 1. For deciduous needleleaf forest, the GEOV2 and GEOV3 FVC products show better consistency with similar frequency distributions. However, the GLASS FVC product has more pixels between 0.65 and 0.9 over deciduous needleleaf forest. For permanent wetlands, the frequencies of the GLASS FVC values between 0.3 and 0.6 are higher than the GEOV2 and GEOV3 values. For closed shrubland and croplands, all three products achieve excellent agreements in the frequency distributions. For grasslands, the GLASS FVC product showed more pixels with low values close to 0. For barren or sparsely vegetated regions, most of the FVC values of these products were less than 0.1.

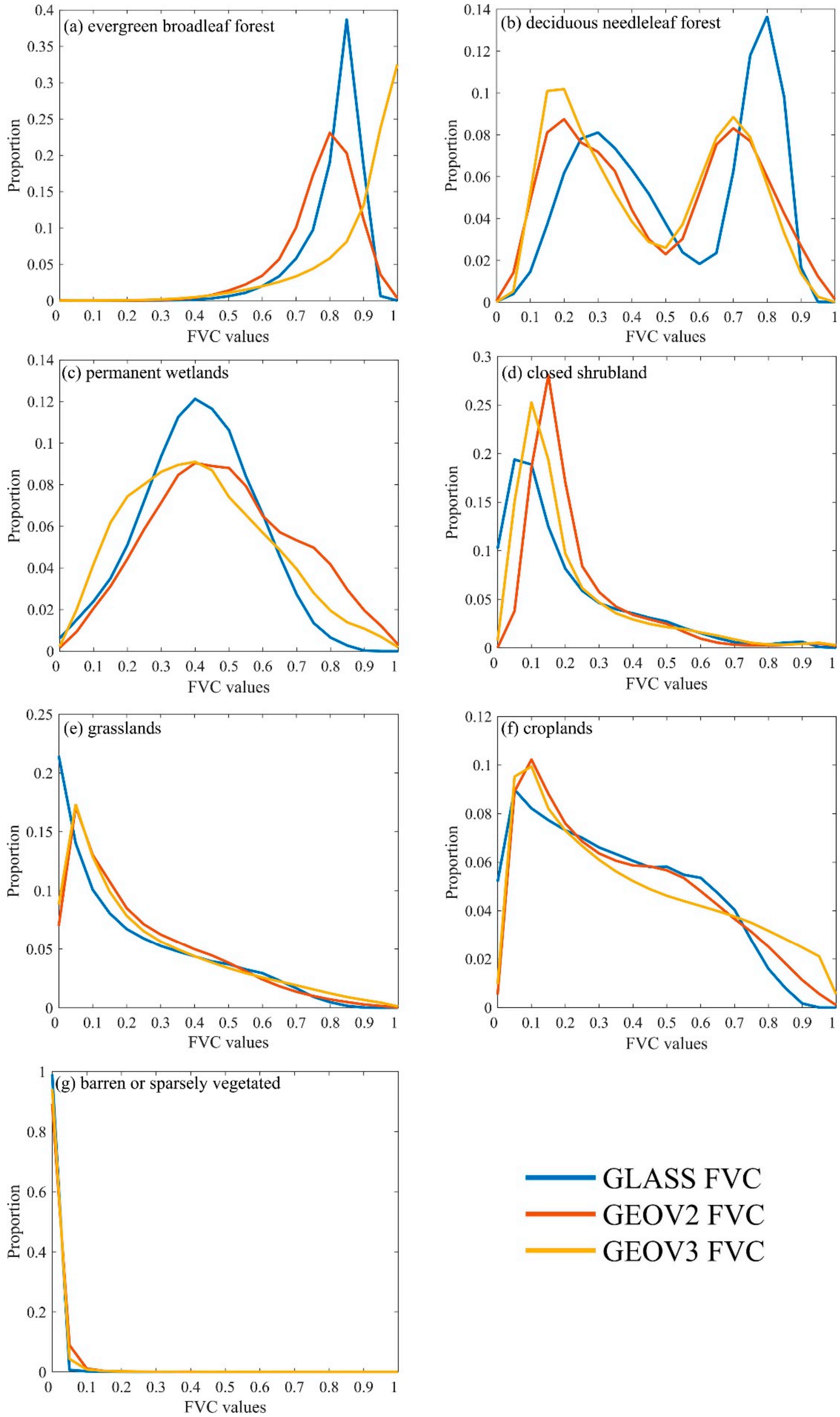


**Figure 3.** Histograms of GEOV2, GEOV3, and GLASS FVC products from 2014 to 2016 with different vegetation types.

## 4.2. Temporal Consistency

To compare the temporal consistency, the mean FVC time series values from the GEOV2 (2001–2016), GEOV3 (2014–2016) and GLASS (2001–2016) FVC products with different vegetation types are shown in Figure 4. By visual observation, the varying magnitude of all the FVC products are coincident with the corresponding vegetation types. For evergreen broadleaf forest, the GLASS and GEOV2 FVC values have stable consistency, showing slight seasonality and maintaining high FVC values throughout the year. However, overall, the GEOV3 FVC values are systematically 0.05 higher than the GLASS and GEOV2 FVC values for evergreen broadleaf forests. For deciduous needleleaf and broadleaf forests, the main discrepancies between GLASS and GEOV2 FVC products occur during the seasons with low FVC values, when the GEOV2 presents clearly smaller FVC values than the GLASS product at valley values. The GEOV3 FVC product shows more agreements with the GEOV2 FVC product over deciduous needleleaf forests. Nevertheless, there is better consistency between the GEOV3 and GLASS products in deciduous broadleaf forests. For closed shrubland and croplands, all three FVC products achieve similar temporal variations and seasonal dynamics. For grasslands, the GEOV3 product presents smaller seasonal dynamics and higher FVC values than both the GEOV2 and GLASS FVC products, which present stable temporal consistency. For barren or sparsely vegetated biomes, all of these products have low inter-annual variations, as expected, and the GEOV2 values were slightly higher than the GLASS values.

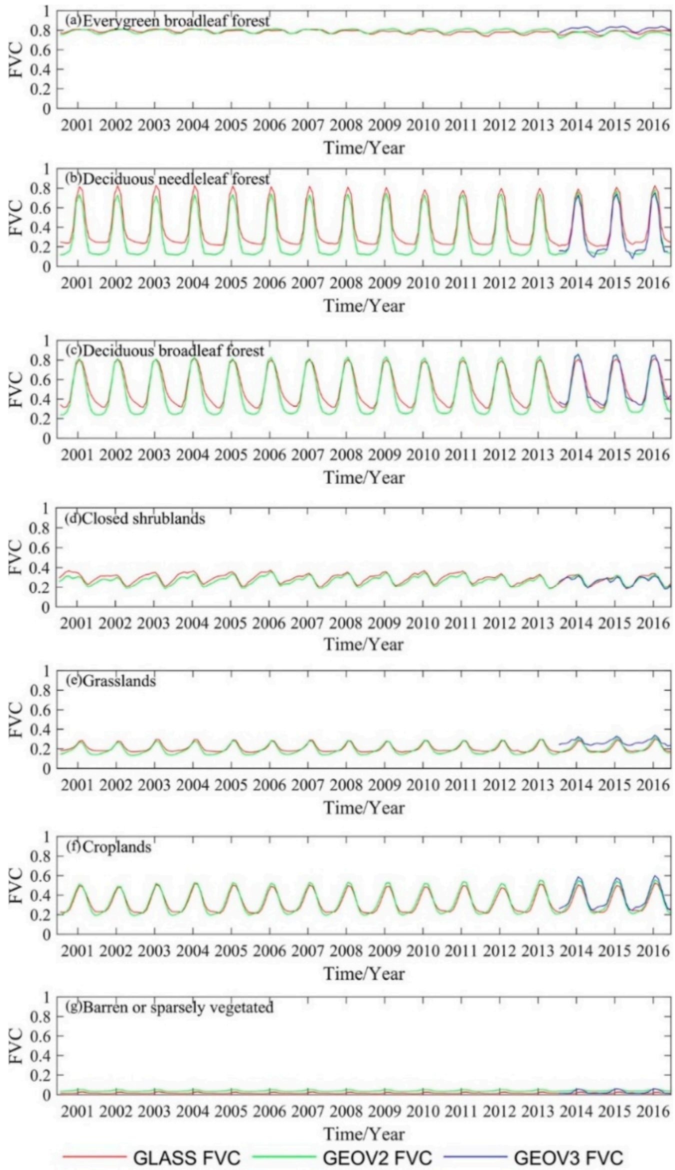


**Figure 4.** Temporal profiles of mean FVC data for GLASS, GEOV2, and GEOV3 FVC products over different vegetation types.

Figure 5 shows the temporal profiles derived from the GEOV2, GEOV3, and GLASS FVC products over the site locations from Table 2. For better visual presentation and comparison, the reference FVC values of the selected sites are exhibited in Figure 5. In Figure 5a,d, both the GEOV2 and GEOV3 products have similar seasonal dynamics and magnitudes, whereas the GLASS FVC values are smaller than those of GEOV2 and GEOV3 for the rice, tree plantation, tea and coffee vegetation types during the growing season. In Figure 5b,f, the GEOV2 and GLASS FVC products achieve reliable agreement in wheat, barley, corn, sunflower and soybean croplands. However, the GEOV3 values are over 0.15 higher than the GEOV2 and GLASS FVC values during summer. Furthermore, all these FVC products demonstrate satisfactory temporal consistency in Figure 5c,e, which are covered by wheat, corn soybean and grass. Generally, all these time series of different FVC products present consistent seasonal dynamics and magnitude ranges with corresponding vegetation types. Obviously, the GEOV2 and GLASS FVC products show complete temporal continuity, whereas the temporal profiles of the GEOV3 FVC product are discontinuous with poor-quality temporal continuity.

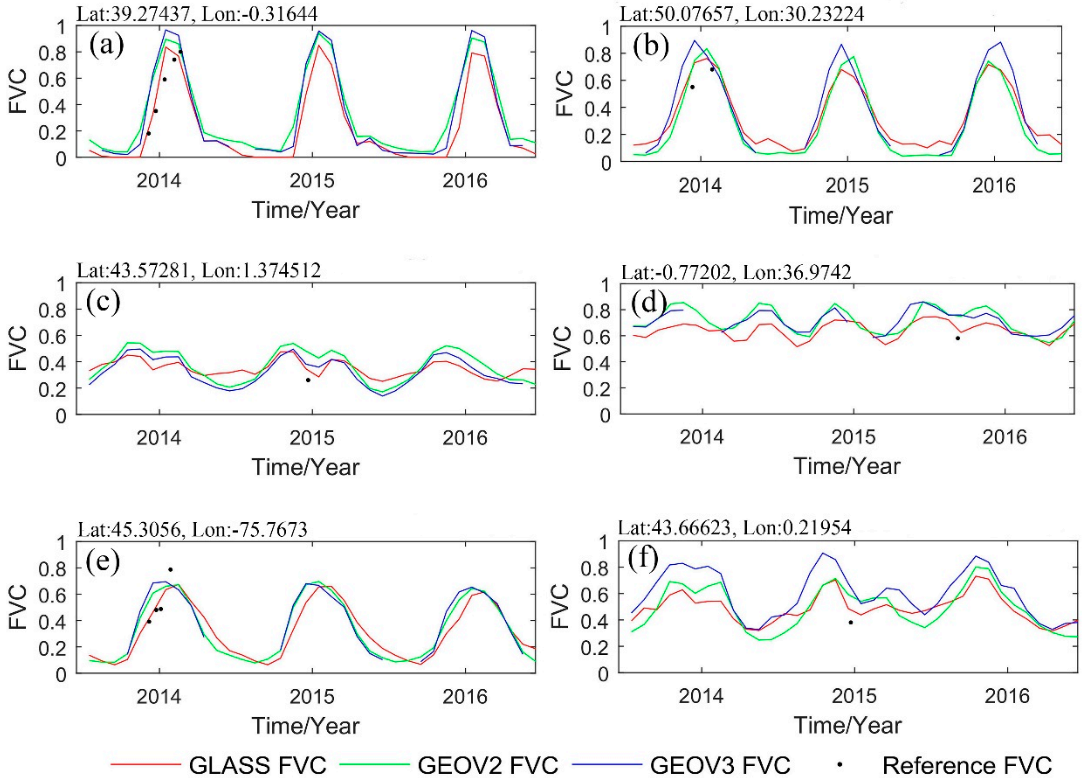


**Figure 5.** Temporal profiles of the GEOV2, GEOV3, and GLASS FVC products. (**a**) Rice. (**b**) Wheat, barley, corn, sunflower, and soybean. (**c**) Grass. (**d**) Tree, tea, and coffee. (**e**) Wheat, corn, and soybean. (**f**) Wheat and sunflower.

### *4.3. Accuracy Validation*

The scatterplots of the three FVC products and the reference FVC values are shown in Figure 6. The RMSE of the reference FVC data is taken as the error bar in Figure 6, which aims to visually indict the uncertainty of reference data. Obviously, the GLASS FVC product has better consistency with the reference data compared with the GEOV2 and GEOV3 FVC data. A regression equation with a 0.7452 slope and a 0.2680 intercept is established between the GEOV2 FVC product and reference FVC values in Figure 6a, which presents high uncertainty and overestimation of small estimations based on the available reference data. In Figure 6b, a clear systematic overestimation (up to approximately 0.2) of the reference data is observed for the GEOV3 FVC product, whose regression equation has a slope of 1.0162 and an intercept of 0.1887 with the reference data. Furthermore, the GLASS FVC product achieves a more reliable accuracy ($R^2$ = 0.7878, RMSE = 0.1212) than the GEOV2 ($R^2$ = 0.5798, RMSE = 0.1921) and GEOV3 FVC data ($R^2$ = 0.7744, RMSE = 0.2224) over the reference FVC values. In addition, considering the uncertainty of the reference FVC values in each field site, there are 8, 3 and 16 sites within the error range of the GEOV2, GEOV3, and GLASS FVC products, respectively. This finding further indicates the better performance of the GLASS FVC product with the available reference FVC data.

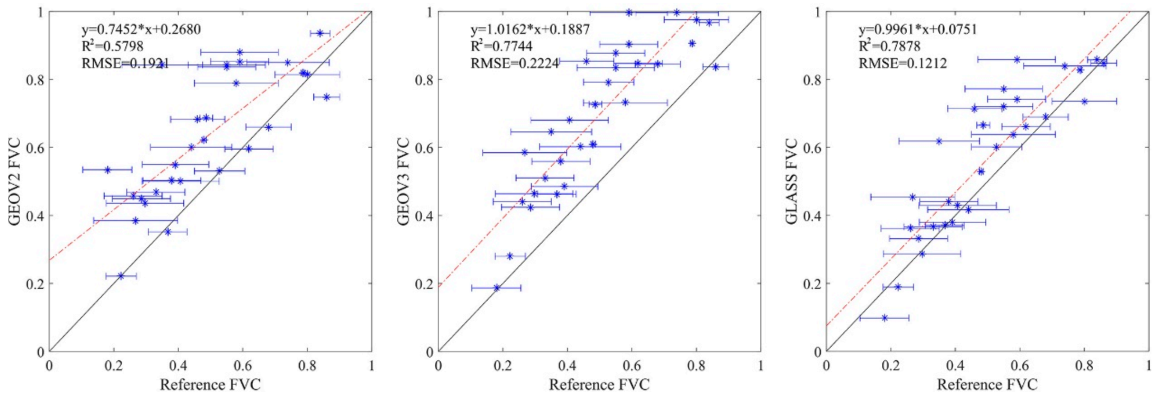


**Figure 6.** Scatterplots between different FVC products and high-spatial resolution reference FVC data.

## 5. Discussion

The comparison and validation for the GEOV2, GEOV3, and GLASS FVC products show that these three global-scale products present satisfying agreements, which have very similar spatiotemporal variations over most areas on a global scale. During the GLASS FVC product generation, a MODIS reflectance re-processing method was developed to obtain the continuous and smooth surface reflectance data by Tang et al [55]. In this method, the contaminated reflectance data were identified through the MODIS quality control data, the temporal characteristics of the spectrum, as well as other auxiliary information, and missing data were filled using an optimum interpolation algorithm [12,55]. With reliable reflectance data, the GLASS FVC product achieved excellent spatial, as well as temporal continuity and completeness. For the GEOV2 FVC product, compositing processes were performed for the FVC estimations instead of the reflectance data, which aimed to reduce the sensitivity of the missing data. Consequently, this strategy tremendously improved the spatial continuity and completeness compared to the GEOV1 FVC product [1,28,53]. For the GEOV3 FVC product, the main reason for the missing data over the high latitudes in winter was the snow coverage and persistent cloudiness, which led to high uncertainty in the PROBA-V reflectance data [56]. Moreover, during the GEOV3 FVC generation, a particular gap-filling method was used over evergreen broadleaf forests because of the large amount of cloud contaminated observations, which might be the main explanation for the overestimation of GEOV3 FVC in equator regions [56,57].

Due to the reprocessing and smoothing processes, both GEOV2 and GLASS FVC products have more agreements and reliable seasonal variations over the most temporal profiles. However, the temporal profiles of the GEOV3 FVC data are slightly noisy in deciduous forests, croplands and grasslands. Because there are no available climatology data, it is difficult to build with limited time series data on a 300-m pixel scale [30]. For accuracy validation, both the GEOV2 and GEOV3 products adopt the corrected CYCLOPES FVC values as training samples. Nevertheless, this procedure may lead to a limitation of accuracy when CYCLOPES FVC do not perform well in some cases [56,57]. Hence, both the GEOV2 and GEOV3 FVC algorithms may need to fine-tune the parameters for high-accuracy estimations. Specifically, real PROBA-V data may be required for neural network training in GEOV3 FVC generation. For the GLASS FVC product, high quality Landsat TM/ETM+ data are used to generate the high-spatial-resolution FVC values as training samples [12]. The sample data are further refined based on the approximate linear relationship between the FVC and NDVI values. With the high-quality sample data, the GLASS FVC product is more reliably accurate in this study.

## 6. Conclusions

In this study, the performances of the three representative and available global-scale FVC time series products, including the GEOV2, GEOV3, and GLASS FVC products, were compared and evaluated for spatiotemporal consistency and accuracy. Based on this study, the following conclusions can be drawn: (1) The GLASS FVC product is much more continuous and complete based on the comparison. Additionally, the GLASS FVC product presents more reliable accuracy by direct comparison against the available reference FVC data ($R^2$ = 0.7878, RMSE = 0.1212). (2) The GEOV2 FVC product shows numerous consistencies with the GLASS FVC product over most regions on a global scale. According to the accuracy validation using the available reference data, high uncertainties are found for low FVC values in the GEOV3 FVC product ($R^2$ = 0.5798, RMSE = 0.1921). (3) The GEOV3 FVC product shows poor performance in the spatiotemporal completeness and continuity. Moreover, systematic overestimation (up to approximately 0.2) is observed in the GEOV3 FVC product compared with the reference FVC values ($R^2$ = 0.7744, RMSE = 0.2224). Additionally, the number of the reference data is small in this study and our further work will focus on extensive validation of these FVC products using reference data with more vegetation types and land surface conditions.

**Author Contributions:** K.J. conceptualized this study; D.L and K.J. made the data curation; D.L., K.J. and X.W. provided the methods of this study; K.J offered the resources; K.J. supervised this study; D.L performed the processes of comparison and validation for adopted FVC products; D.L wrote this paper; K.J., X.W., X.Z., M.X., Y.Y., X.Z. and B.W. reviewed and edited this paper.

**Funding:** This research was funded by the National Key Research and Development Program of China under grant numbers 2016YFA0600103 and 2016YFB0501404, the National Natural Science Foundation of China under grant number 41671332, the Open Fund of Key Laboratory of Geospatial Technology for the Middle and Lower Yellow River Regions (Henan University), Ministry of Education under grant numbers GTYR201806 and the Tang Scholar Program (Kun Jia is a Tang Scholar of Beijing Normal University).

**Acknowledgments:** The authors would like to thank the anonymous reviewers and editors for their valuable comments and suggestions that have significantly improved this paper.

**Conflicts of Interest:** The authors declare no conflict of interest.

## Appendix A

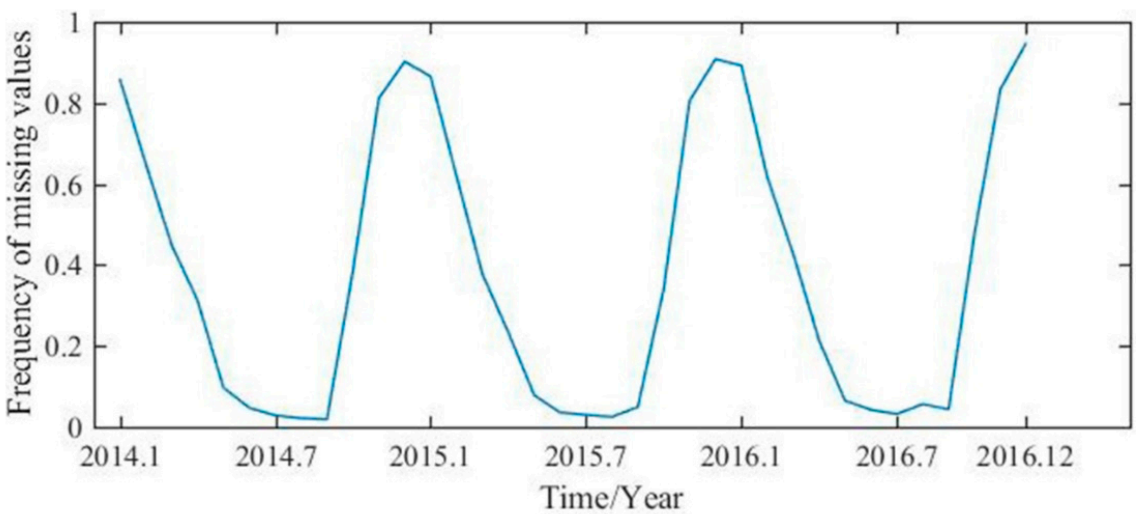


**Figure A1.** Frequency of missing values for evergreen needle forest in GEOV3 FVC product during 2014 to 2016.

Figure A1 showed the frequency of missing value over evergreen needle forest in GEOV3 FVC product during 2014 to 2016. Obviously, there were approximately 50% of missing data within half a year over evergreen needle forest in GEOV3 FVC product. Considering the massive missing data of GEOV3 FVC product over evergreen needle forests, it was reasonable to drop this vegetation type for further evaluation.

## References

1. Camacho, F.; Cernicharo, J.; Lacaze, R.; Baret, F.; Weiss, M. GEOV1: LAI, FAPAR essential climate variables and FCOVER global time series capitalizing over existing products. Part 2: Validation and intercomparison with reference products. *Remote Sens. Environ.* **2013**, *137*, 310–329. [CrossRef]
2. Zhang, X.; Liao, C.; Li, J.; Sun, Q. Fractional vegetation cover estimation in arid and semi-arid environments using HJ-1 satellite hyperspectral data. *Int. J. Appl. Earth Obs. Geoinform.* **2013**, *21*, 506–512. [CrossRef]
3. Jia, K.; Liang, S.; Gu, X.; Baret, F.; Wei, X.; Wang, X.; Yao, Y.; Yang, L.; Li, Y. Fractional vegetation cover estimation algorithm for Chinese GF-1 wide field view data. *Remote Sens. Environ.* **2016**, *177*, 184–191. [CrossRef]
4. Godínez-Alvarez, H.; Herrick, J.; Mattocks, M.; Toledo, D.; Van Zee, J. Comparison of three vegetation monitoring methods: Their relative utility for ecological assessment and monitoring. *Ecol. Indic.* **2009**, *9*, 1001–1008. [CrossRef]
5. Gutman, G.; Ignatov, A. The derivation of the green vegetation fraction from NOAA/AVHRR data for use in numerical weather prediction models. *Int. J. Remote Sens.* **1998**, *19*, 1533–1543. [CrossRef]
6. Jiménez-Muñoz, J.; Sobrino, J.; Plaza, A.; Guanter, L.; Moreno, J.; Martínez, P. Comparison between fractional vegetation cover retrievals from vegetation indices and spectral mixture analysis: Case study of PROBA/CHRIS data over an agricultural area. *Sensors* **2009**, *9*, 768–793. [CrossRef] [PubMed]
7. Yang, L.; Jia, K.; Liang, S.; Liu, J.; Wang, X. Comparison of four machine learning methods for generating the GLASS fractional vegetation cover product from MODIS data. *Remote Sens.* **2016**, *8*, 682. [CrossRef]
8. Wu, D.; Wu, H.; Zhao, X.; Zhou, T.; Tang, B.; Zhao, W.; Jia, K. Evaluation of spatiotemporal variations of global fractional vegetation cover based on GIMMS NDVI data from 1982 to 2011. *Remote Sens.* **2014**, *6*, 4217–4239. [CrossRef]
9. Zeng, X.; Dickinson, R.E.; Walker, A.; Shaikh, M.; DeFries, R.S.; Qi, J. Derivation and evaluation of global 1-km fractional vegetation cover data for land modeling. *J. Appl. Meteorol.* **2000**, *39*, 826–839. [CrossRef]
10. Xiao, J.; Moody, A. A comparison of methods for estimating fractional green vegetation cover within a desert-to-upland transition zone in central New Mexico, USA. *Remote Sens. Environ.* **2005**, *98*, 237–250. [CrossRef]
11. Bioucas-Dias, J.M.; Plaza, A.; Dobigeon, N.; Parente, M.; Du, Q.; Gader, P.; Chanussot, J. Hyperspectral unmixing overview: Geometrical, statistical, and sparse regression-based approaches. *IEEE J. Sel. Top. Appl. Earth Obs. Remote Sens.* **2012**, *5*, 354–379. [CrossRef]
12. Jia, K.; Liang, S.; Liu, S.; Li, Y.; Xiao, Z.; Yao, Y.; Jiang, B.; Zhao, X.; Wang, X.; Xu, S. Global land surface fractional vegetation cover estimation using general regression neural networks from MODIS surface reflectance. *IEEE Trans. Geosci. Remote Sens.* **2015**, *53*, 4787–4796. [CrossRef]
13. Jiapaer, G.; Chen, X.; Bao, A. A comparison of methods for estimating fractional vegetation cover in arid regions. *Agric. For. Meteorol.* **2011**, *151*, 1698–1710. [CrossRef]
14. Adams, J.B.; Smith, M.O.; Johnson, P.E. Spectral mixture modeling: A new analysis of rock and soil types at the Viking Lander 1 site. *J. Geophys. Res. Solid Earth* **1986**, *91*, 8098–8112. [CrossRef]
15. Zou, J.; Lan, J.; Shao, Y. A hierarchical sparsity unmixing method to address endmember variability in hyperspectral image. *Remote Sens.* **2018**, *10*, 738. [CrossRef]
16. Shao, Y.; Lan, J.; Zhang, Y.; Zou, J. Spectral unmixing of hyperspectral remote sensing imagery via preserving the intrinsic structure invariant. *Sensors* **2018**, *18*, 3528. [CrossRef] [PubMed]
17. Roujean, J.L.; Lacaze, R. Global mapping of vegetation parameters from POLDER multiangular measurements for studies of surface-atmosphere interactions: A pragmatic method and its validation. *J. Geophys. Res. Atmos.* **2002**, *107*, ACL–6. [CrossRef]
18. Roujean, J.L.; Leroy, M.; Deschamps, P.Y. A bidirectional reflectance model of the Earth's surface for the correction of remote sensing data. *J. Geophys. Res. Atmos.* **1992**, *97*, 20455–20468. [CrossRef]

19. García-Haro, F.; Camacho, F.; Verger, A.; Meliá, J. Current status and potential applications of the LSA SAF suite of vegetation products. Proceedings of 29th EARSeL Symposium, Chania, Greece, 15–18 June 2009.
20. García-Haro, F.; Sommer, S.; Kemper, T. Variable multiple endmember spectral mixture analysis (VMESMA): A high performance computing and environment analysis tool. *Remote Sens. Environ.* **2001**. ready for submission.
21. García-Haro, F.; Camacho-de Coca, F.; Meliá, J.; Martínez, B. Operational derivation of vegetation products in the framework of the LSA SAF project. In Proceedings of the 2005 EUMETSAT Meteorological Satellite Conference, Dubrovnik, Croatia, 19–23 September 2005; pp. 19–23.
22. Baret, F.; Hagolle, O.; Geiger, B.; Bicheron, P.; Miras, B.; Huc, M.; Berthelot, B.; Niño, F.; Weiss, M.; Samain, O. LAI, fAPAR and fCover CYCLOPES global products derived from VEGETATION: Part 1: Principles of the algorithm. *Remote Sens. Environ.* **2007**, *110*, 275–286. [CrossRef]
23. Verger, A. Analisi comparativa d'algorismes operacionals d'estimacio de parametres biofisics de la coberta vegetal amb teledeteccio. Ph.D. Thesis, Universitat de Valencia, Valencia, Spain, 2008.
24. Ding, Y.; Zheng, X.; Jiang, T.; Zhao, K. Comparison and validation of long time serial global geov1 and regional Australian modis fractional vegetation cover products over the Australian continent. *Remote Sens.* **2015**, *7*, 5718–5733. [CrossRef]
25. Baret, F.; Weiss, M.; Lacaze, R.; Camacho, F.; Makhmara, H.; Pacholcyzk, P.; Smets, B. GEOV1: LAI and FAPAR essential climate variables and FCOVER global time series capitalizing over existing products. Part1: Principles of development and production. *Remote Sens. Environ.* **2013**, *137*, 299–309. [CrossRef]
26. Fillol, E.; Baret, F.; Weiss, M.; Dedieu, G.; Demarez, V.; Gouaux, P.; Ducrot, D. Cover fraction estimation from high resolution SPOT HRV & HRG and medium resolution SPOT-VEGETATION sensors. Validation and comparison over South-west France. In Proceedings of the Second International Symposium on Recent Advances in Quantitative Remote Sensing, Torrent, Valencia, Spain, 25–29 September 2006; pp. 25–29.
27. Mu, X.; Huang, S.; Ren, H.; Yan, G.; Song, W.; Ruan, G. Validating GEOV1 fractional vegetation cover derived from coarse-resolution remote sensing images over croplands. *IEEE J. Sel. Top. Appl. Earth Obs. Remote Sens.* **2015**, *8*, 439–446. [CrossRef]
28. Verger, A.; Baret, F.; Weiss, M. GEOV2/VGT: Near real time estimation of global biophysical variables from VEGETATION-P data. In Proceedings of the MultiTemp 2013: 7th International Workshop on the Analysis of Multi-temporal Remote Sensing Images, Banff, AB, Canada, 25–27 June 2013; pp. 1–4.
29. Verger, A.; Baret, F.; Weiss, M. Algorithm Theorethical Basis Document of GEOV2 FVC. Available online: https://land.copernicus.eu/global/sites/cgls.vito.be/files/products/CGLOPS1_ATBD_FCOVER1km-V2_I1.41.pdf (accessed on 22 September 2019).
30. Baret, F.; Weiss, M.; Verger, A.; Smets, B. ATBD for LAI, FAPAR and FCOVER from PROBA-V products at 300m resolution (GEOV3). Available online: https://land.copernicus.eu/global/sites/cgls.vito.be/files/products/ImagineS_RP2.1_ATBD-FCOVER300m_I1.73.pdf (accessed on 22 September 2019).
31. Camacho, F.; Sánchez, J.; Lacaze, R.; Weiss, M.; Baret, F.; Verger, A.; Smets, B.; Latorre, C. Validating GEOV3 LAI, FAPAR and vegetation cover estimates derived from PROBA-V observations at 333m over Europe. In Proceedings of the EGU General Assembly Conference Abstracts, Vienna, Austria, 17–22 April 2016.
32. Jia, K.; Yang, L.; Liang, S.; Xiao, Z.; Zhao, X.; Yao, Y.; Zhang, X.; Jiang, B.; Liu, D. Long-term Global Land Surface Satellite (GLASS) fractional vegetation cover product derived from MODIS and AVHRR Data. *IEEE J. Sel. Top. Appl Earth Obs. Remote Sens.* **2019**, *12*, 508–518. [CrossRef]
33. García-Haro, F.J.; Camacho-de Coca, F.; Miralles, J.M. Inter-comparison of SEVIRI/MSG and MERIS/ENVISAT biophysical products over Europe and Africa. In Proceedings of the 2nd MERIS/(A) ATSR User Workshop, Frascati, Italy, 22–26 September 2008; pp. 22–26.
34. Xiao, Z.; Wang, T.; Liang, S.; Sun, R. Estimating the fractional vegetation cover from GLASS leaf area index product. *Remote Sens.* **2016**, *8*, 337. [CrossRef]
35. Baret, F.; Pavageau, K.; Béal, D.; Weiss, M.; Berthelot, B.; Regner, P. *Algorithm Theoretical Basis Document for MERIS Top of Atmosphere Land Products (TOA_VEG)*; INRA-CSE: Avignon, France, 2006.
36. Baret, F.; Weiss, M.; Verger, A.; Kandasamy, S. *BioPar Methods Compendium-LAI, FAPAR and FCOVER from LTDR AVHRR Series*; INRA-EMMAH: Avignon, France, 2011.
37. Verger, A.; Baret, F.; Weiss, M. Performances of neural networks for deriving LAI estimates from existing CYCLOPES and MODIS products. *Remote Sens. Environ.* **2008**, *112*, 2789–2803. [CrossRef]

38. Baret, F.; Morissette, J.T.; Fernandes, R.A.; Champeaux, J.L.; Myneni, R.B.; Chen, J.; Plummer, S.; Weiss, M.; Bacour, C.; Garrigues, S. Evaluation of the representativeness of networks of sites for the global validation and intercomparison of land biophysical products: Proposition of the CEOS-BELMANIP. *IEEE Trans. Geosci. Remote Sens.* **2006**, *44*, 1794–1803. [CrossRef]
39. Maisongrande, P.; Duchemin, B.; Dedieu, G. VEGETATION/SPOT: An operational mission for the Earth monitoring; presentation of new standard products. *Int. J. Remote Sens.* **2004**, *25*, 9–14. [CrossRef]
40. Verger, A.; Baret, F.; Weiss, M. A multisensor fusion approach to improve LAI time series. *Remote Sens. Environ.* **2011**, *115*, 2460–2470. [CrossRef]
41. Verger, A.; Baret, F.; Weiss, M.; Kandasamy, S.; Vermote, E. The CACAO method for smoothing, gap filling, and characterizing seasonal anomalies in satellite time series. *IEEE Trans. Geosci. Remote Sens.* **2013**, *51*, 1963–1972. [CrossRef]
42. Dierckx, W.; Sterckx, S.; Benhadj, I.; Livens, S.; Duhoux, G.; Van Achteren, T.; Francois, M.; Mellab, K.; Saint, G. PROBA-V mission for global vegetation monitoring: Standard products and image quality. *Int. J. Remote Sens.* **2014**, *35*, 2589–2614. [CrossRef]
43. Liang, S.; Zhang, X.; Xiao, Z.; Cheng, J.; Liu, Q.; Zhao, X. *Global LAnd Surface Satellite (GLASS) products: Algorithms, Validation and Analysis*; Springer Science & Business Media: Berlin, Germany, 2013.
44. Liang, S.; Zhao, X.; Liu, S.; Yuan, W.; Cheng, X.; Xiao, Z.; Zhang, X.; Liu, Q.; Cheng, J.; Tang, H.; et al. A long-term Global LAnd Surface Satellite (GLASS) data-set for environmental studies. *Int. J. Dig. Earth* **2013**, *6*, 5–33. [CrossRef]
45. Jia, K.; Liang, S.; Wei, X.; Yao, Y.; Yang, L.; Zhang, X.; Liu, D. Validation of Global LAnd Surface Satellite (GLASS) fractional vegetation cover product from MODIS data in an agricultural region. *Remote Sens. Lett.* **2018**, *9*, 847–856. [CrossRef]
46. Camacho, F.; Lacaze, R.; Latorre, C.; Baret, F.; De la Cruz, F.; Demarez, V.; Di Bella, C.; García-Haro, J.; González-Dugo, M.P.; Kussul, N. Collection of ground biophysical measurements in support of copernicus global land product validation: The ImagineS database. *Geophys. Res. Abstr.* **2015**, *17*, EGU2015–2209.
47. Morisette, J.T.; Baret, F.; Privette, J.L.; Myneni, R.B.; Nickeson, J.E.; Garrigues, S.; Shabanov, N.V.; Weiss, M.; Fernandes, R.A.; Leblanc, S.G. Validation of global moderate-resolution LAI products: A framework proposed within the CEOS land product validation subgroup. *IEEE Trans. Geosci. Remote Sens.* **2006**, *44*, 1804–1817. [CrossRef]
48. Friedl, M.A.; Sulla-Menashe, D.; Tan, B.; Schneider, A.; Ramankutty, N.; Sibley, A.; Huang, X. MODIS Collection 5 global land cover: Algorithm refinements and characterization of new datasets. *Remote Sens. Environ.* **2010**, *114*, 168–182. [CrossRef]
49. Sulla-Menashe, D.; Friedl, M.A. *User Guide to Collection 6 MODIS Land Cover (MCD12Q1 and MCD12C1) Product*; USGS: Reston, VA, USA, 2018.
50. Xiao, Z.; Liang, S.; Sun, R. Evaluation of three long time series for global fraction of absorbed photosynthetically active radiation (FAPAR) products. *IEEE Trans. Geosci. Remote Sens.* **2018**, *56*, 5509–5524. [CrossRef]
51. Prajapati, A.; Naik, S.; Mehta, S. Evaluation of different image interpolation algorithms. *Int. J. Comput. Appl.* **2012**, *58*, 6–12. [CrossRef]
52. Verger, A.; Baret, F.; Weiss, M. Near real-time vegetation monitoring at global scale. *IEEE J. Sel. Top. Appl Earth Obs. Remote Sens.* **2014**, *7*, 3473–3481. [CrossRef]
53. Smets, B.; Verger, A.; Camacho, F.; Goten, R.V.d.; Jacobs, T. Product User Manual for GEOV2 Products. Available online: https://land.copernicus.eu/global/sites/cgls.vito.be/files/products/CGLOPS1_PUM_FCOVER1km-V2_I1.33.pdf (accessed on 22 September 2019).
54. Olson, D.M.; Dinerstein, E.; Wikramanayake, E.D.; Burgess, N.D.; Powell, G.V.; Underwood, E.C.; D'amico, J.A.; Itoua, I.; Strand, H.E.; Morrison, J.C. Terrestrial ecoregions of the world: A new map of life on earth: A new global map of terrestrial ecoregions provides an innovative tool for conserving biodiversity. *BioScience* **2001**, *51*, 933–938. [CrossRef]
55. Tang, H.; Yu, K.; Hagolle, O.; Jiang, K.; Geng, X.; Zhao, Y. A cloud detection method based on a time series of MODIS surface reflectance images. *Int. J. Dig. Earth* **2013**, *6*, 157–171. [CrossRef]

56. Smets, B.; Jacobs, T.; Verger, A. Product User Manual for GEOV3 Products. Available online: https://land.copernicus.eu/global/sites/cgls.vito.be/files/products/GIOGL1_PUM_FCOVER300m-V1_I1.60.pdf (accessed on 22 September 2019).
57. Sánchez-Zapero, J.; Fuster, B.; Camacho, F. Quality Assessment Report for GEOV3 Products. Available online: https://land.copernicus.eu/global/sites/cgls.vito.be/files/products/CGLOPS1_QAR_FCOVER300-V1_I2.00.pdf (accessed on 22 September 2019).